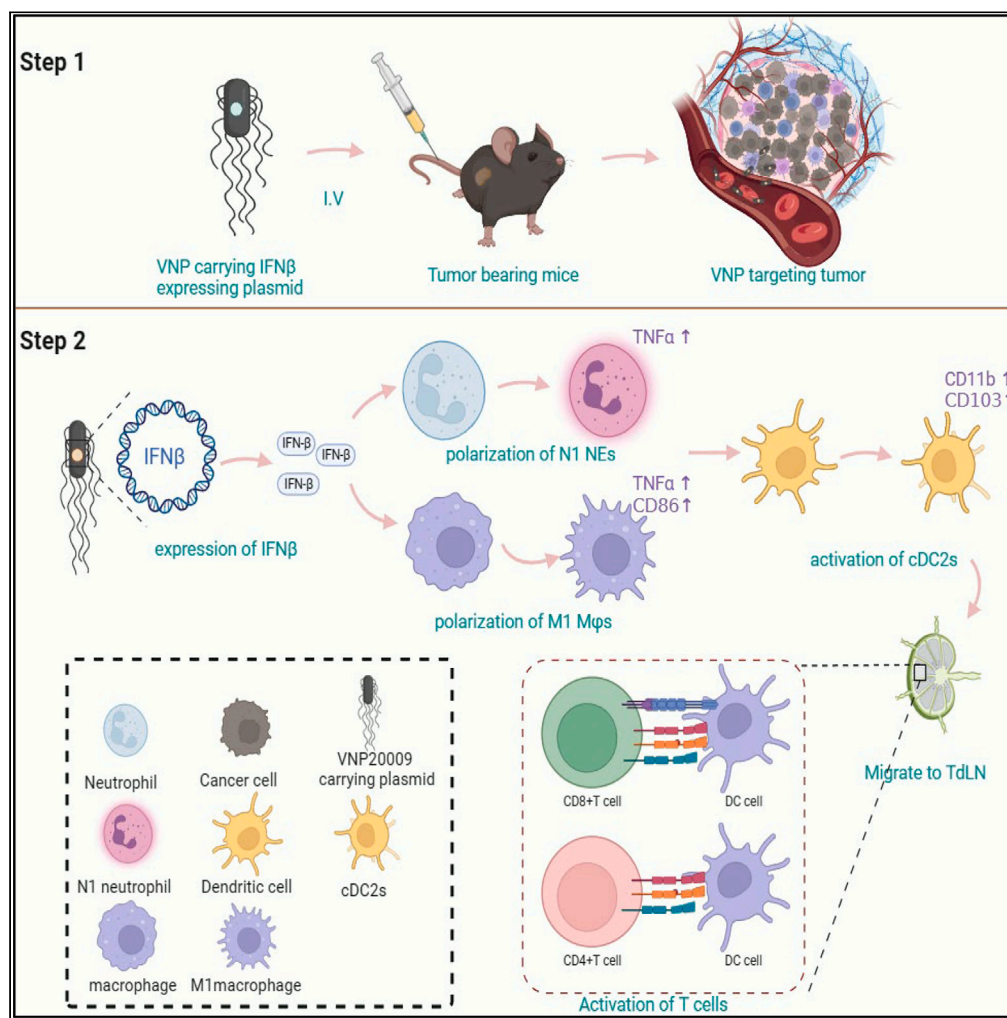


Article

Oncolytic bacteria VNP20009 expressing IFN β inhibits melanoma progression by remodeling the tumor microenvironment



Lina Liu, Qiang Li, Chen Chen, Wenjie Xin, Chao Han, Zichun Hua

zchua@nju.edu.cn

Highlights

Bacteria-mediated delivery system (VNP-IFN β) continuously secret IFN- β in tumor

VNP-IFN β inhibit the subcutaneous tumor progression and lung metastasis

VNP-IFN β directly induce tumor apoptosis

VNP-IFN β induce macrophages polarization, DCs mature and T cells activation

Liu et al., iScience 27, 109372
April 19, 2024 © 2024 The Authors. Published by Elsevier Inc.
<https://doi.org/10.1016/j.isci.2024.109372>



Article

Oncolytic bacteria VNP20009 expressing IFN β inhibits melanoma progression by remodeling the tumor microenvironmentLina Liu,^{1,4} Qiang Li,^{1,4} Chen Chen,¹ Wenjie Xin,¹ Chao Han,¹ and Zichun Hua^{1,2,3,5,*}

SUMMARY

In the tumor microenvironment (TME), tumor-associated NEs (TANs) have the potential to be protumorigenic or antitumorigenic within the TME in response to environmental cues. The diversity and plasticity of NEs (NEs) underlie the dual potential of TANs in the TME. Here, we utilized the tumor-targeting bacterium VNP20009 (VNP) to carry a plasmid expressed IFN β (VNP-IFN β), which can deliver IFN β and remodel TANs to an antitumorigenic phenotype, and performed preclinical evaluations in the B16F10 lung metastasis model and the B16F10 subcutaneous xenograft model. Compared with VNP, VNP-IFN β recruited more NEs and macrophages (M ϕ s) with antitumor phenotypes in lung metastases and activated dendritic cells (DCs) differentiation, which activated antitumor immune responses of CD4⁺ T cells, and ultimately inhibited melanoma progression. This study enriches the bacterial-mediated tumor therapy by using tumor-targeting bacteria to deliver IFN β to the tumor site and inhibit melanoma growth and metastasis by remodeling the tumor immune microenvironment.

INTRODUCTION

The tumor microenvironment (TME) is an integral part of cancer, acting as a complex ecosystem that supports tumor growth and metastatic dissemination while attenuating immunosurveillance.¹ Considerable efforts have been made to remodel TME for cancer therapy such as targeting tumor-infiltrating T-cells via immune checkpoint blockade,² normalizing blood vessels through anti-angiogenic therapy³ and reprogramming of tumor-associated macrophages (TAMs) to restore antitumor properties.⁴ NEs (NEs), which act as the first line of defense in innate immunity, constitute an important component of TME and are actively involved in tumor progression and metastasis.⁵ Tumor-associated NEs (TANs) exert dual function in cancer. Specifically, while TANs have been reported to be tumor-promoting in genetically engineered mouse models (GEMMs) of cancer,⁶ it also engaged in the process of antitumor resistance by interacting with other immune cells or killing tumor cells directly.⁷ This dual function reveals the potential which TANs can be remodeled to perform only antitumor functions. TANs can be polarized to antitumor (N1-like) or protumor (N2-like) phenotypes.⁸ N1 NEs can inhibit tumor growth by increasing immune recognition of cancer cells through neutrophil-dependent upregulation of self-antigen presentation⁹ and inhibit metastatic seeding in the lungs through generation of H₂O₂.¹⁰ Interferon- β (IFN β) was reported to polarize TANs into the anti-tumor N1 phenotype in both mice and in human cancer patients.¹¹ Compared with control mice, mice with impaired type I IFN signaling (Ifnar1^{-/-}) develop more lung metastases in the 4T1 mammary and LLC lung carcinoma model.¹² Altogether, these results indicate that IFN- β may have significant therapeutic potential. As a kind of protein drugs, IFN- β is commonly administered subcutaneously, which avoids first-pass effects and has high bioavailability. However, protein drugs are administered in limited dosages in a single subcutaneous dose, resulting in insufficient persistence.¹³ Given that protein drugs are easily degraded, many strategies for sustained-release protein drugs have been proposed such as moderating the degradation of drugs through the introduction of organic vehicles or agarose hydrogels.^{14,15}

Recently, genetically engineered oncolytic bacteria have attracted wide attentions as tumor-targeting drug delivery system in cancer therapy. Compared with conventional drug delivery systems, such as liposomes, micelles and nanoparticles (NPs), bacteria-based delivery systems have superior advantages, including: (1) Unlike liposomes, micelles, and NPs, which can only be passively targeted to tumors via blood transport, oncolytic bacteria can actively target TME and proliferate in the tumor,¹⁶ due to reduced immune surveillance along with the hypoxic and necrotic tumor core environment. (2) Oncolytic bacteria can be genetically engineered to carry prokaryotic expression vectors, acting as "drug factories" to express therapeutic proteins, such as anti-PD1 nanobody¹⁷ or anti-TNF- α nanobody,¹⁸ *in situ* in

¹The State Key Laboratory of Pharmaceutical Biotechnology, School of Life Sciences; Nanjing University, Nanjing 210023, Jiangsu, China

²Changzhou High-Tech Research Institute of Nanjing University and Jiangsu, Changzhou, Jiangsu 213164, China

³TargetPharma Laboratories Inc, Changzhou 213164, Jiangsu, China

⁴These authors contributed equally

⁵Lead contact

*Correspondence: zchua@nju.edu.cn

<https://doi.org/10.1016/j.isci.2024.109372>



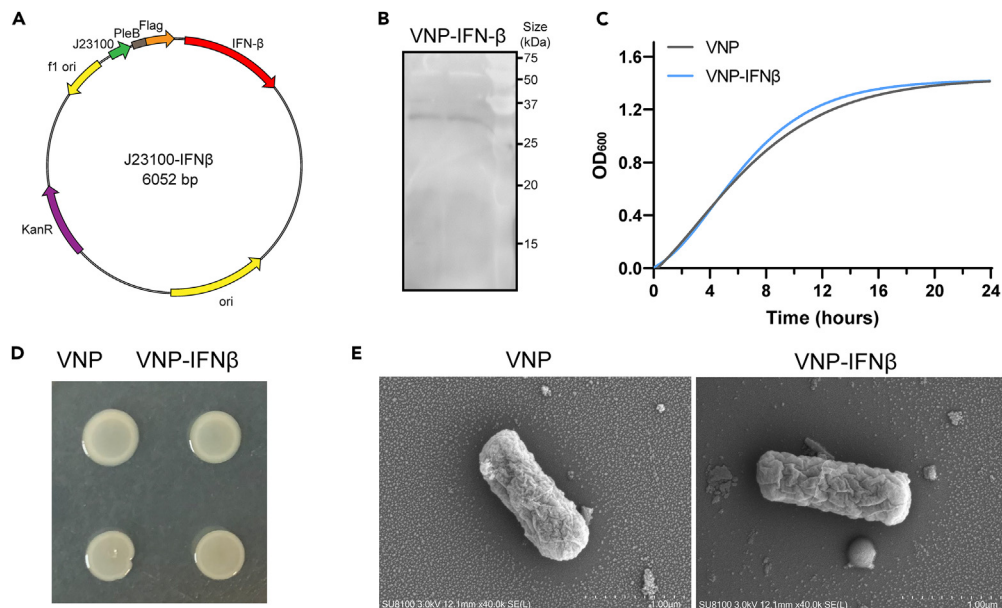


Figure 1. Construction and characterization of VNP-IFN β

- (A) Schematic diagram of the pJ23100-IFN β plasmid.
 (B) The expression of IFN β in VNP after electroporation was analyzed via western blot.
 (C) Bacteria growth curves of VNP and VNP-IFN β (n=6).
 (D) Colonial morphology of VNP and VNP-IFN β .
 (E) Scanning electron microscopes (SEM) of VNP and VNP-IFN β .

the tumor, avoiding the metabolism or degradation of the drug in plasma while avoiding toxicity resulting from systemic drug administration. (3) Since engineered bacteria can proliferate in tumors, a single administration enables sustained release of therapeutic proteins in tumor. Attenuated *Salmonella typhimurium* VNP20009 (VNP), which was deleted *purl* and *msbB* gene to reduce immune stimulation and further improve targeting ability,¹⁹ is one of the most potential strains. Furthermore, as the only strain in *Salmonella* evaluated in clinical trial, VNP has been widely used in drug delivery including carrying plasmids expressing therapeutic proteins such as anti-PD1 nanoantibodies or interferon- γ ,^{17,20} cytotoxic protein,^{21,22} cytokines or immune-modulators,^{23,24} tumor vaccine,²⁵ or expressing shRNA against cancer-promoting genes.²⁶

In this study, we report the generation of a recombinant VNP strain that expresses the IFN β protein (VNP-IFN β). VNP-IFN β is capable of targeting melanoma and inhibiting tumor growth while maintaining a certain biosafety. In addition, it can profoundly remodel the TME in lung metastases and activate CD4⁺T cell-mediated antitumor responses to suppress melanoma lung metastasis.

RESULTS

Construction and characterization of VNP-IFN β

To obtain recombinant VNP strains that can stably express and secrete IFN β , PelB signal peptide was fused to the N-terminus of the protein to realize the secretion of IFN β and FLAG tag was inserted into the N-terminus of the protein to facilitate subsequent analyses (Figure 1A). Western blot result verified that the strain expressed IFN β (Figure 1B). To further determine whether the expression of IFN β affects bacterial reproduction, the growth curve of VNP and VNP-IFN β were monitored (Figure 1C) and the result indicated that expressed IFN β does not affect the proliferation of VNP. In addition, the colony morphology and the morphology of individual bacteria cell was detected by scanning electron microscopy (SEM) (Figures 1D and 1E). These results revealed that the normal morphology of bacteria was not affected after the transformation of IFN β expression plasmid into VNP.

VNP-IFN β stimulates NEs and M ϕ s activation *in vitro*

In order to analyze the effect of VNP-IFN β on the polarization of neutrophils (NEs), we co-incubated 4×10^5 primary NEs with VNP-IFN β for 1.5h, and analyzed the expression levels of N1 markers and N2 markers via qPCR. The results showed that the N1-like markers of NEs were significantly upregulated (Figure 2A) and the N2-like markers were significantly downregulated (Figure 2B) after VNP-IFN β stimulation, which suggests that VNP-IFN β can induce NEs polarization to the N1 phenotype *in vitro*.

Macrophages (M ϕ s) account for a large proportion (about 50%) in the TME²⁷ and play an important role in immunosuppression. Numerous studies in bacterial-mediated tumor therapy effectively reverse tumor immunosuppression and significantly enhances the effect of tumor

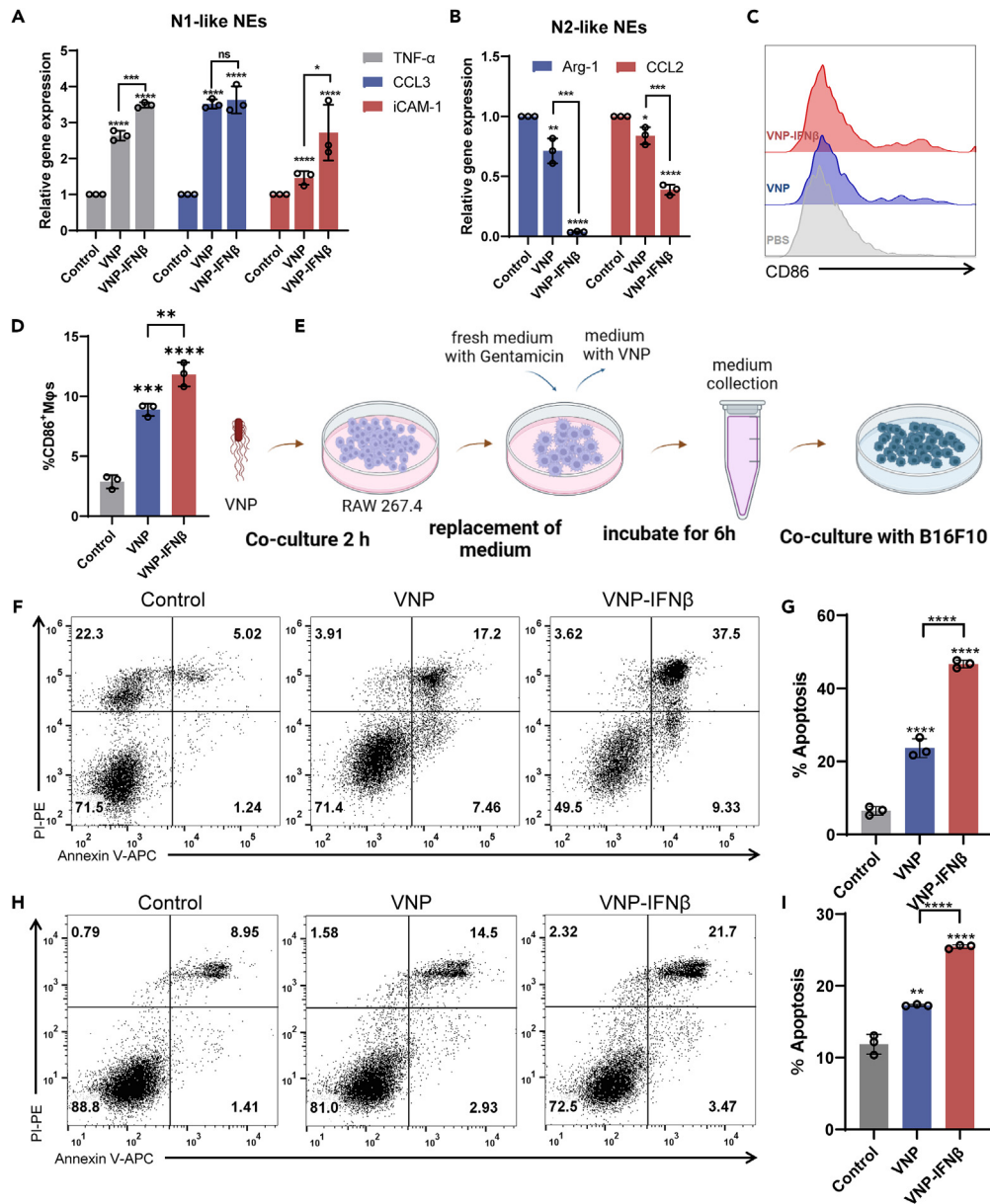


Figure 2. VNP-IFN β stimulates NEs and M ϕ s activation in vitro

(A and B) The expression of N1 (A) and N2 (B) phenotypic markers of NEs after VNP-IFN β stimulation was analyzed via qPCR.

(C and D) The expression of CD86 of RAW264.7 cells after VNP-IFN β stimulation was analyzed via FACS.

(E) Schematic diagram of apoptosis induced in B16F10 cells by supernatants of RAW264.7 cell medium after VNP-IFN β stimulation.

(F and G) The apoptosis levels of B16F10 cells after incubated for 16 h with the culture supernatant of RAW264.7 cells, which was stimulated with VNP, VNP-IFN β , or not (n=3).

(H and I) The apoptosis levels of B16F10 cells after incubated with VNP, VNP-IFN β , or not (n=3). Data are shown as the mean \pm SD. ****p < 0.0001, ***p < 0.001, **p < 0.01, *p < 0.05, ns: no significance.

immunotherapy by polarizing TAMs to the M1 type.^{17,28,29} Therefore, we examined the polarization phenotype of RAW264.7 cells after VNP-IFN β stimulation via flow cytometry *in vitro*, and the results showed that the expression level of CD86 in RAW264.7 cells was much higher than that in the PBS group (11.8% vs. 2.9%) and the VNP group (11.8% vs. 8.9%) (Figures 2C and 2D), which suggests that VNP-IFN β can promote the macrophage polarization to M1 antitumor phenotype. Next, we examined the expression levels of different polarization markers of RAW264.7 cells after VNP-IFN β stimulation via RT-PCR *in vitro*. The results showed that the expression of M1-like polarization markers including *TNF- α* , *IFN- γ* , and *iNOS* were upregulated (Figure S1A) while that of M2-like polarization markers, *FIZZ1*, was downregulated (Figure S1B). Those

results suggested that VNP-IFN β can effectively stimulate RAW264.7 cells to M1-like phenotype polarization and inhibit its polarization to M2-like phenotype.

Moreover, we co-cultured the supernatant of stimulated RAW264.7 cells medium with B16F10 cells to analyze the anti-tumor effect of RAW264.7 cells after VNP-IFN β stimulation (Figure 2E), results revealed that the apoptosis percentage of the VNP-IFN β group was up to 46% which was much higher than that in the control group and the VNP group (Figures 2F and 2G). This indicated that RAW264.7 cells exhibited stronger tumor killing ability after VNP-IFN β stimulation. While directly co-incubating B16F10 cells with VNP and VNP-IFN β , the apoptosis rate of B16F10 cells in the VNP group and the VNP-IFN β group were still higher than that of the control. In addition, compared with the VNP group, the VNP-IFN β treatment induced a significant increase of apoptosis rate of B16F10 cells approximately 1.5 times (Figures 2H and 2I), indicating that VNP-IFN β has direct killing effect on tumor cells.

Taken together, VNP-IFN β can effectively stimulate the activation of NEs and RAW264.7 cells to antitumor phenotype and exert antitumor effects by expressing IFN β , meanwhile, have a direct tumor-killing ability.

VNP-IFN β inhibits melanoma growth and metastasis

To visualize the distribution of VNP-IFN β in tumors, we constructed a VNP-IFN β -mCherry recombinant strain. Fluorescence microscopy imaging results (Figure S2A) and Western blot assay (Figure S2B) verified the expression of IFN β -mCherry. To further determine the expression of IFN β -mCherry in recombinant strain, we measured the relative fluorescence intensity of different concentrations of IFN β -mCherry (Figure S2C) and found that the fluorescence intensity of 107 VNP-IFN β -mCherry was comparable to that of 6 μ g IFN β -mCherry protein. To demonstrate the superiority of VNP delivery system, 107 VNP-IFN β -mCherry and 6 μ g IFN β -mCherry protein were *i.v.* administered to B16F10 subcutaneous xenograft model, respectively, and the fluorescence signals in the tumors site were detected at different time (Figures S2D, and S2E). The results showed that fluorescence signals of IFN β -mCherry protein and VNP-IFN β -mCherry could be detected in tumors 2 h after administration. The fluorescence intensity of IFN β -mCherry peaked at 6 h after administration, and then began to gradually diminish, whereas the fluorescence signal of VNP-IFN β -mCherry continued to rise, and the signal intensity of VNP-IFN β -mCherry was 5 times higher than that of the IFN β -mCherry 24 h after administration, suggesting that VNP-IFN β -mCherry has a superior tumor retention capability.

After validating the immunostimulatory effect of VNP-IFN β on RAW264.7 cells *in vitro*, we further explored its antitumor effect *in vivo*. Unilateral B16F10 tumor-bearing mice model were treated following the therapeutic schedule (Figure 3A), then separated the mice randomly into three groups and treated with PBS, VNP and VNP-IFN β . As the results showed, VNP and VNP-IFN β had excellent tumor-targeting ability, and the titer of bacteria colonized in the tumor was approximately 1000 times higher than that in the other organs (Figure 3B). In addition, the VNP-IFN β group exhibited the strongest inhibition of tumor growth (Figures 3C and 3D), the average tumor volume of the mice treated with VNP-IFN β was less than 250 mm³, whereas that of the PBS groups are more than 1500 mm³. Besides, VNP-IFN β treatment significantly prolonged the survival time of mice (Figure 3E). Certain antitumor effect of VNP was also observed in our study, which is attribute to the nutrient competition caused by bacterial growth as well as immune activation induced by bacteria. The above results verified that VNP-IFN β could inhibit effectively inhibit melanoma growth.

Type I IFNs were reported to interfere with the formation of the pre-metastatic niche in the lung and with NEs polarization, leading to an anti-metastatic phenotype¹² and consequently inhibit the formation of lung metastatic foci. Therefore, a B16F10 lung metastasis mouse model was established to explore the potential of VNP-IFN β inhibiting tumor metastasis. Tumor-bearing mice were treated as the scheme described (Figure 3F). As the results showed (Figures 3G and 3H), the number of B16F10 lung metastases in the VNP-IFN β group was significantly reduced compared with that in the PBS group and VNP group. This result suggested that VNP-IFN β administration inhibited the lung metastasis of melanoma.

In conclusion, VNP-IFN β exhibited excellent inhibition of melanoma lung metastasis and melanoma growth *in vivo*.

VNP-IFN β exhibits favorable biosafety *in vivo*

Bacteria mediated cancer therapy leads to tumor-bearing mouse's losing weight and hepatosplenomegaly after administration, which were identified as side effects of bacteria therapy.³⁰ Based on that, the safety of VNP-IFN β *in vivo* needs further assessment. In the B16F10 lung metastasis model, C57BL/6J mice were divided into 3 groups and injected *i.v.* with PBS, VNP, and VNP-IFN β , then monitored body weight daily and executed the mice on day 5. Compared with the VNP group, the VNP-IFN β group showed a lower degree of body weight loss in the first few days after administration (Figures 4A, and S3A), suggesting that VNP-IFN β has less systemic toxicity, as body weight is the main indicator of systemic toxicity.^{31–33} However, hepatosplenomegaly did not resolve in the VNP-IFN β group compared with the VNP group (Figures 4B and 4C), implying that VNP-IFN β administration leads to hepatosplenomegaly injury. Serological analysis further showed that the serum levels of ALT, AST were increased in the VNP-IFN β group compared with the VNP group (Figures 4D and 4E), which was associated with the nonspecific expression of IFN β in the liver by VNP-IFN β . Specifically, IFN β secreted by VNP-IFN β could induce a pro-inflammatory response,³⁴ regulates chemokine secretion, leads to infiltration of immune cells in the liver, and induces an increase in the secretion of inflammatory factors such as TNF α , IL-11, 1L-6, and nitric oxide (NO),³⁵ which can lead to certain toxic side effects. Meanwhile, the levels of BUN and Scr did not change significantly (Figures 4F and 4G), suggesting that VNP-IFN β caused slight liver damage, but not kidney damage. In addition, the H&E staining results showed that VNP-IFN β did not cause significant organic changes (Figure 4H).

In summary, we concluded that VNP-IFN β not only effectively inhibited melanoma metastasis, but also had a favorable biosafety profile.

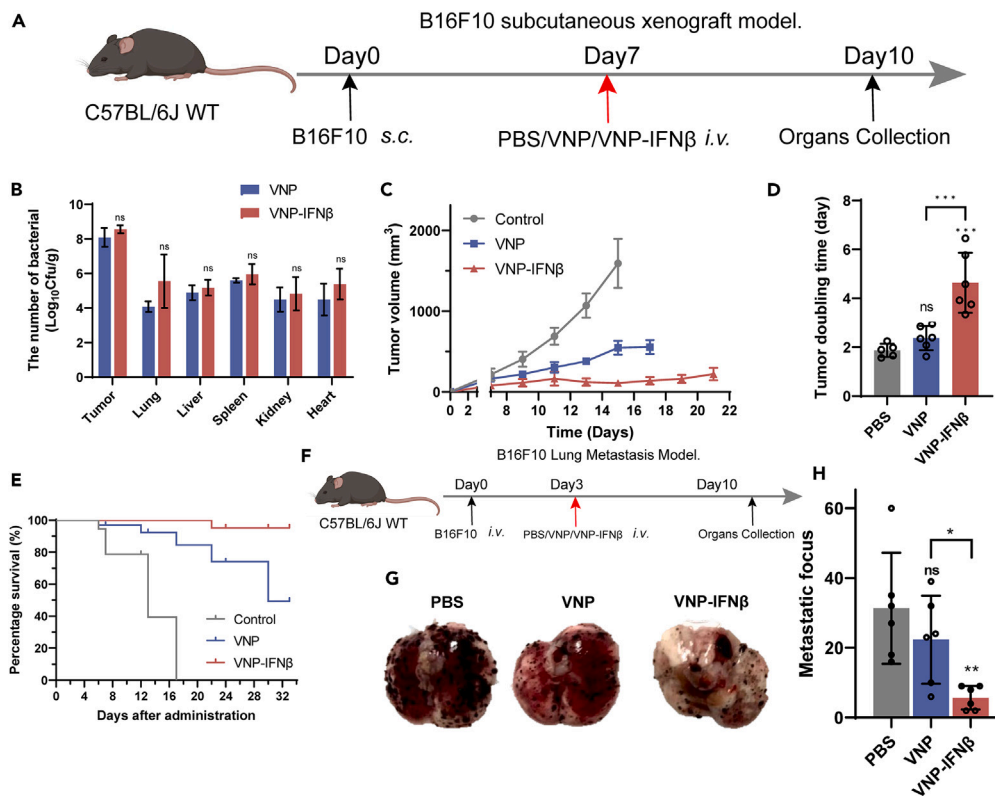


Figure 3. VNP-IFN β inhibits tumor growth and metastasis

(A) The treatments schedule for VNP-IFN β inhibition of tumor growth in subcutaneous xenograft model: 7 days after B16F10 cells injection, PBS, VNP, VNP-IFN β were administrated by intravenous (*i.v.*) and the tissues were collected at 10 days.
 (B) Bacterial titers in different organs after drug administration in B16F10 subcutaneous xenograft model ($n=3$).
 (C–E) The tumor growth curve, tumor doubling time and survival curve of B16F10 subcutaneous xenograft model ($n=6$).
 (F) The treatments schedule for VNP-IFN β inhibition of tumor metastasis in B16F10 lung metastasis model: 3 days after B16F10 cells injection, PBS, VNP, VNP-IFN β were administrated by *i.v.* and the tissues were collected at 10 days.
 (G and H) The pictures and numbers of the lung metastasis foci in B16F10 lung metastasis model ($n=6$). Data are shown as the mean \pm SD. **** $p < 0.0001$, *** $p < 0.001$, ** $p < 0.01$, * $p < 0.05$, ns: no significance.

VNP-IFN β promotes antitumor polarization of NEs and M ϕ s

Tumor infiltrating leukocytes, i.e., M ϕ s and NEs, a significant population of immune cells that infiltrate tumor tissue, were shown to be involved in tumor growth and play a significant role in the prognosis of cancer patients.³⁶ Therefore, we investigated the tumor infiltrating leukocytes in metastases to reveal the mechanism of VNP-IFN β inhibition of tumor growth and metastasis.

The infiltration rates of NEs in lung metastases were 9.5% and 27.1% in the VNP and VNP-IFN β groups, which were 2.3-fold and 6.6-fold higher than that in the PBS group, respectively (Figures 5A and 5B). The increased NEs infiltration in the VNP group was associated with bacterial-mediated activation of innate immunity,³⁷ whereas the more increased infiltration of NEs in the VNP-IFN β group indicated that the additional increase in NEs was recruited via expressed IFN β , which was corroborated by increased NEs in the spleen (Figure S3B). Meta-analyses have shown that high neutrophil/lymphocyte ratio in solid tumors is correlated with poor patient outcome.³⁸ However, this result does not confirm that NEs are responsible for tumor progression. This was confirmed by the results of the present study that both treatment groups recruited more NEs to the metastases compared to the PBS group, but still showed some inhibition of metastasis. Indeed, the high plasticity of NEs endows them with the ability to play different roles in the TME. It has been demonstrated in mouse models that TANs are able to acquire different phenotypes based on specific features of the TME. NEs are polarized to a pro-tumorigenic phenotype (N2) in a TGF β -rich environment, whereas in the presence of IFN β or inhibition of TGF β signaling, NEs are transformed to an N1 phenotype associated with anti-tumorigenic properties.³⁹ Therefore, further analysis of the phenotype of NEs infiltrated in tumors is needed.

Based on that, we further analyzed the proportion of TNF- α ⁺NEs (N1-like antitumor phenotype NEs) in each group. As shown in Figures 5E and 5F, the proportion of TNF- α ⁺NEs was the highest (36%) in the VNP-IFN β group, which was about twice as high as that in the PBS group (19%) and the VNP group (17.6%). This suggests that the VNP-IFN β administration not only recruits more NEs in metastases, but also remodels them to an anti-tumor phenotype.

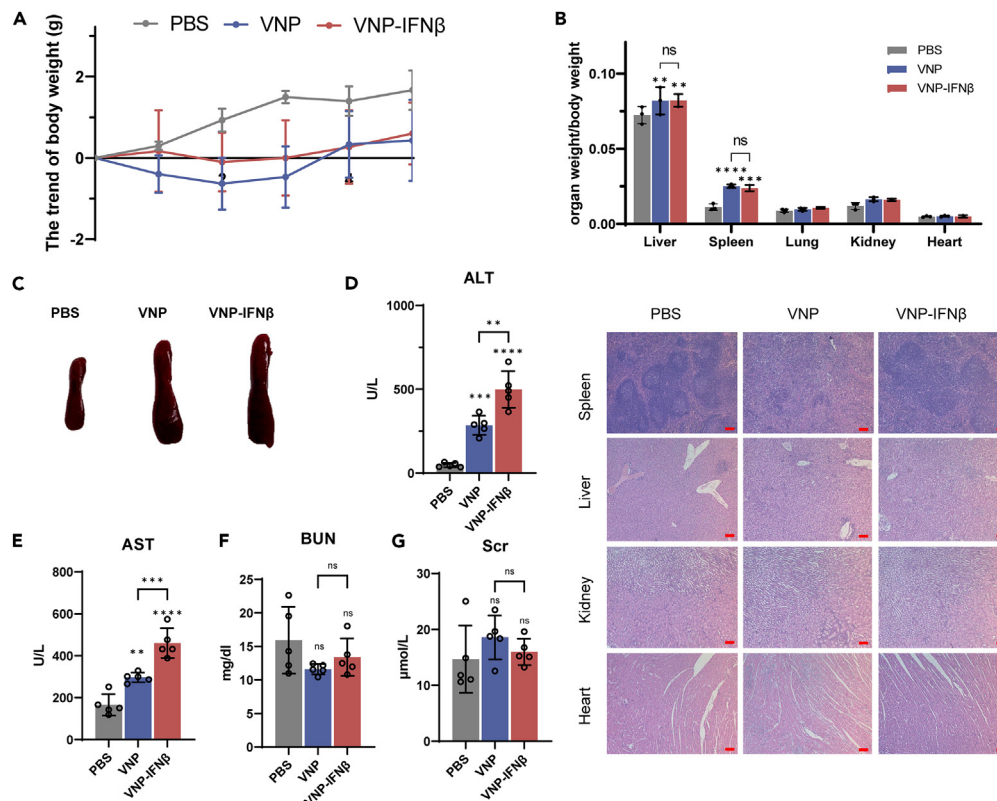


Figure 4. VNP-IFN β exhibits favorable biosafety in vivo

(A) The changing trend of body weight of mouse was monitored daily after treatments (n=6).

(B) The ratio of organ weight to body weight of mouse in the different groups (n=3).

(C) The picture of spleen 5 days after administrations.

(D–G) Serological analysis of ALT (D), AST (E), BUN (F), and Scr (G) in peripheral blood serum 5 days after administration (n=5).

(H) H&E staining of organs in the different groups. Scale bars: 200 μ m. Data are shown as the mean \pm SD. ****p < 0.0001, ***p < 0.001, **p < 0.01, *p < 0.05, ns: no significance.

Analysis of the proportion of infiltrated M ϕ s in metastases and its polarization status yielded similar results. The proportion of infiltrated M ϕ s in the VNP-IFN β group was 45.0%, which was significantly higher than that in the PBS group (23.2%) and in the VNP group (31.0%) (Figures 5C and 5D). Moreover, 25.1% of M ϕ s recruited by VNP-IFN β were TNF- α ⁺ M ϕ s (M1 antitumor phenotype M ϕ s), which was 3 times higher than 8.5% in the PBS group, and 2.6-fold higher than that in the VNP group (9.8%) (Figures 5G and 5H). The above results suggest that, compared with the PBS and VNP group, VNP-IFN β treatment can recruit more M ϕ s in metastases and also enhance the infiltration rate of M1-like antitumor phenotype M ϕ s. In addition, we analyzed the M ϕ s subtypes in peripheral blood and tumor-draining lymph nodes (TdLNs), and found that CD86⁺ M ϕ s in peripheral blood was slightly higher in the VNP-IFN β group compared with the PBS group (6.7% vs. 4.9%), and twice as much as that in the VNP group (6.7% vs. 3.3%) (Figures S3C, and S3D). The infiltration rate of CD86⁺ M ϕ s in TdLNs in the VNP-IFN β group reached 20.2%, which was significantly higher than that in the PBS group (12%) and the VNP group (15.3%) (Figures S3E and S3F). CD86 is considered as a marker of M1-like M ϕ s,⁴⁰ and these results above suggested that VNP-IFN β administration also promotes the polarization of M ϕ s toward an M1-like antitumor phenotype in the periphery and TdLNs, contributing to the inhibition of melanoma growth and metastasis.

Taken all these into consideration, we conclude that after VNP-IFN β treatment, M ϕ s and NEs are mobilized and the levels of M1-like M ϕ s and N1-like NEs in the metastases and peripheral tumor-associated immune organs are significantly increased, which helps to explain the anti-metastatic effect of VNP-IFN β .

VNP-IFN β activates antigen presentation by tumor-infiltrating DCs, thereby activating the antitumor immune response

DCs, a major component of the tumor immune landscape, are the professional antigen-presenting cells (APCs) responsible for activating and maintaining the tumor-specific cytotoxicity of T cells,⁴¹ which can effectively promote antitumor immunity. Analysis of the proportion and subtype of DCs infiltrated in the periphery or tumor helps to illustrate the anti-metastatic mechanism of VNP-IFN β . As shown in Figures 6A and 6B, the tumor infiltration rate of DCs in the VNP-IFN β group was 10.6%, which was significantly higher than 6.5% in the PBS group and 6.9% in the

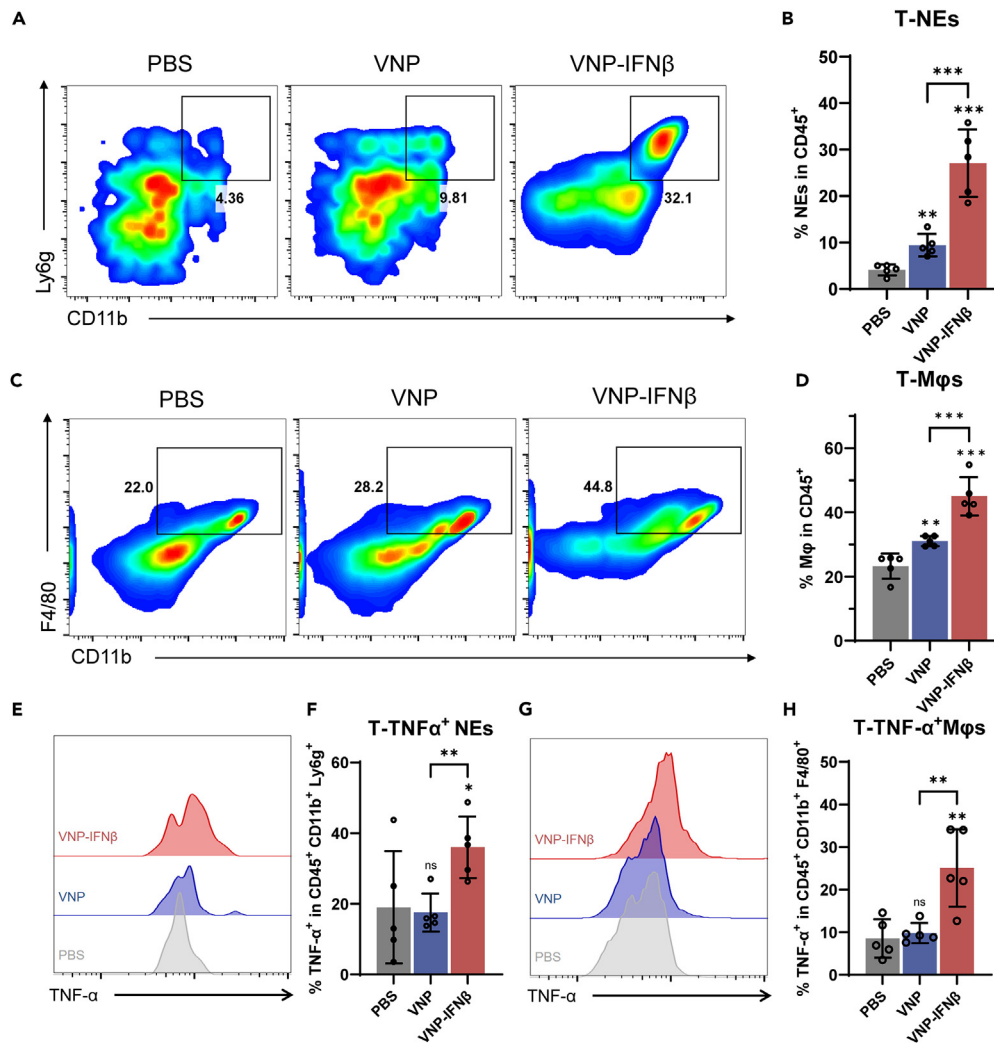


Figure 5. VNP-IFN β stimulates antitumor polarization of NEs and M ϕ s in tumors

(A and B) The percentage of tumor-infiltrating NEs in each group, 5 days after treatments and the statistic diagrams were shown in (B).

(C and D) The percentage of tumor-infiltrating M ϕ s in each group, and the statistic diagrams were shown in (D).

(E and F) The FACS histogram plot and statistic diagrams of TNF- α ⁺ cells in tumor-infiltrating NEs.

(G and H) The FACS histogram plot and statistic diagrams of TNF- α ⁺ cells in tumor-infiltrating M ϕ s. Data are shown as the mean \pm SD. **** p < 0.0001, *** p < 0.001, ** p < 0.01, * p < 0.05, ns: no significance.

VNP group. Similarly, the proportion of DCs in the peripheral blood in the VNP-IFN β group was also 2.2-fold higher than that in the PBS group and 1.7-fold higher than that in the VNP group (Figures S4A and S4B). In addition, the proportion of tumor-associated migratory DCs (CD103⁺ DCs) in peripheral blood in the VNP-IFN β group was also significantly elevated compared with the other two groups (Figures S4C and S4D), and these results indicated that VNP-IFN β administration can recruit more DCs in metastases.

Specifically, conventional dendritic cells (cDC) are divided into two distinct subsets, cDC1s (CD8 α ⁺ and/or CD103⁺ subset) and cDC2s (CD11b⁺ subset).⁴² They stimulate cytotoxic T lymphocyte (CTL) responses and antitumor CD4⁺ T cell responses, respectively.^{42–44} We analyzed the subtypes of DCs infiltrated in the metastases via FACS and found that the infiltration rate of CD11b⁺ DCs in VNP-IFN β metastases was 13.8%, which was significantly higher compared with 5.2% in the PBS group and 8.1% in the VNP group (Figure 6C and 6D), which suggests increased cDC2s infiltration in metastases, and similar results were observed in spleen (Figures S4E and S4F). As we mentioned before, cDC2s are essential for inducing CD4⁺ T cell-mediated immunity in cancer, and the above results imply that VNP-IFN β may achieve inhibition of metastasis by activating CD4⁺ T cell immunity in metastases.

Furthermore, the status of CD8⁺ T cells and CD4⁺ T cells in metastatic foci and TdLNs were evaluated. In the metastatic foci of the VNP-IFN β group, the proportion of infiltrated CD8⁺ T cells was 6.9%, which was significantly decreased compared to 11.3% in the PBS group and 10.4% in the VNP group (Figures S5A and S5B). Meanwhile, the proportion of infiltrating CD4⁺ T cells in the VNP-IFN β metastases was 28.7%

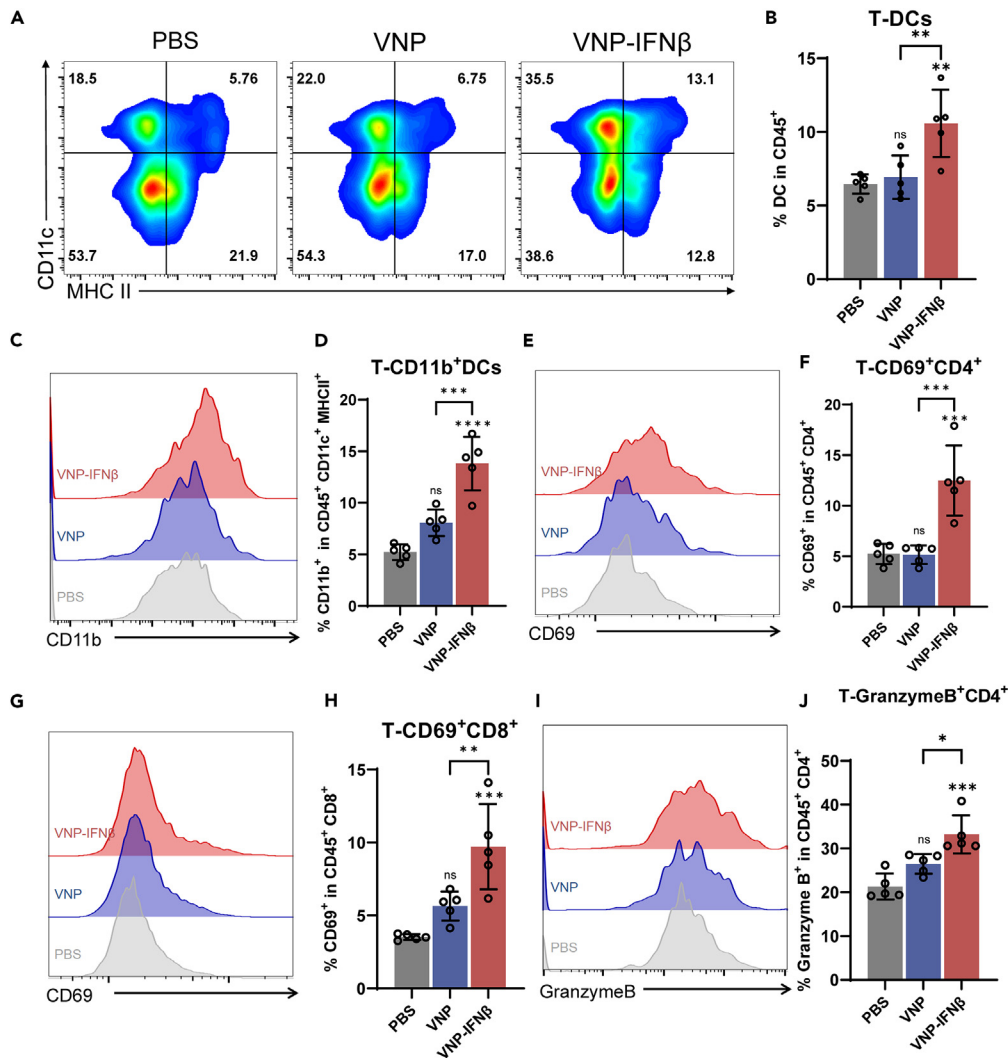


Figure 6. VNP-IFN β activates antigen presentation and antitumor immune response

(A and B) The percentage of tumor-infiltrating DCs in each group and the statistic diagrams were shown in (B).

(C and D) The percentage of CD11b⁺ cells in tumor-infiltrating DCs.

(E and F) The percentage of CD69⁺ CD4⁺ T cells in tumor was analyzed via FACS.

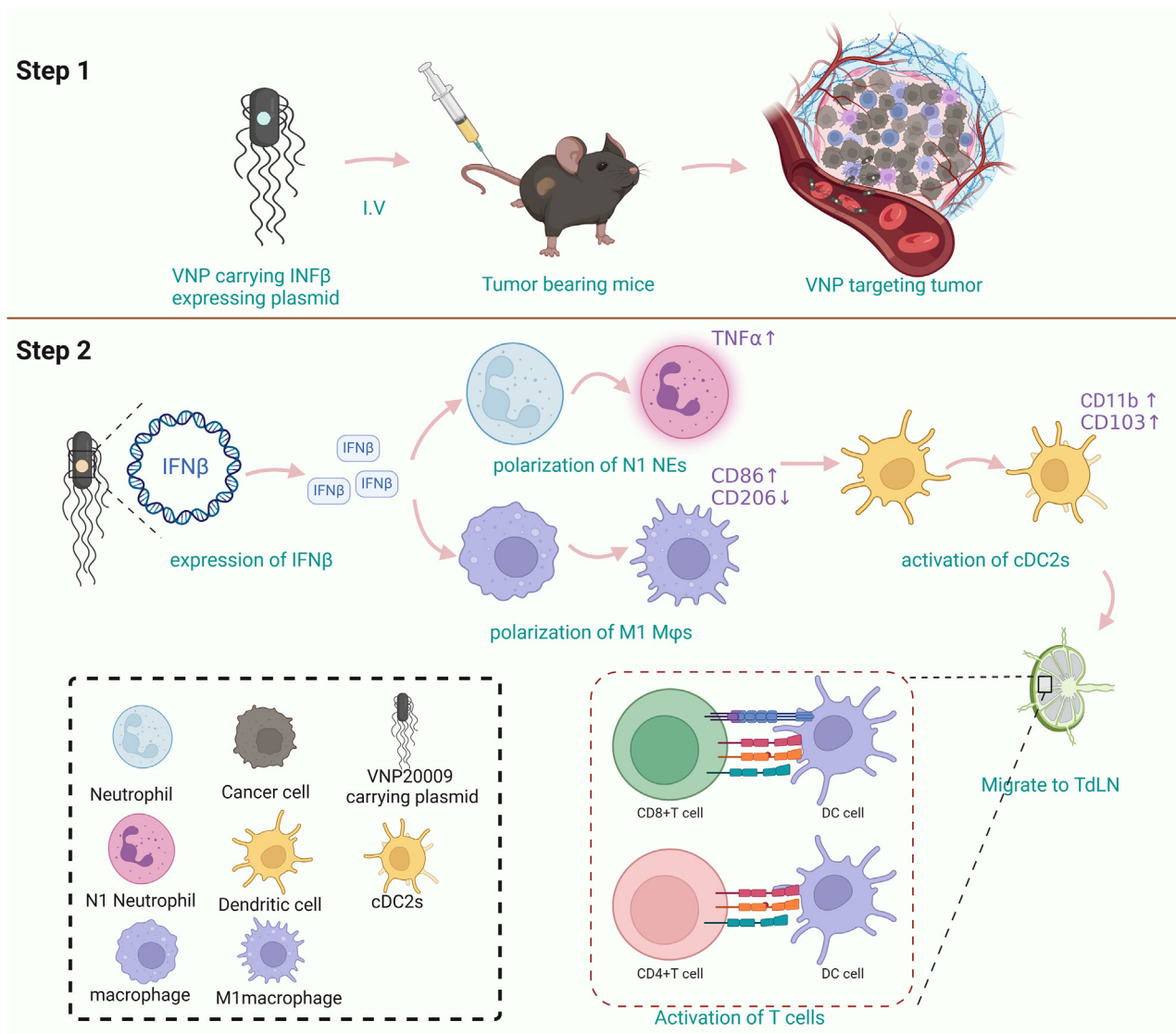
(G and H) The percentage of CD69⁺ CD8⁺ T cells in tumor was analyzed via FACS.

(I and J) The percentage of Granzyme B⁺ CD4⁺ T cells in each group and the statistic diagrams were shown in (J). Data are shown as the mean \pm SD.

****p < 0.0001, ***p < 0.001, **p < 0.01, *p < 0.05, ns: no significance.

(Figure S5C), which showed no significant difference with the PBS group (28.0%) and the VNP group (34.8%), indicating the predominance of CD4⁺ T cells in VNP-IFN β metastatic foci. To further evaluate the activation status of tumor-infiltrating T cells, the expression level of CD69, considered a marker of T cell activation, was analyzed.⁴⁵ As shown in Figures 6E, and 6F, the expression of CD69 in CD4⁺ T cells in the VNP-IFN β group was significantly higher than that in the PBS group (12.5% vs. 5.2%) and the VNP group (12.5% vs. 5.2%), and similar trend was also observed in the expression of CD69 in CD8⁺ T cells (Figure 6G, and 6H), suggesting that VNP-IFN β stimulated the activation of T cells. In addition, the proportion of cytotoxic T cells was evaluated after administration, which was represented by high expression of Granzyme B. As shown in Figures 6I and 6J, the infiltration rate of granzyme B⁺ CD4⁺ T cells in the VNP-IFN β group was 33.2%, which was significantly increased compared to 21.3% in the PBS group and 26.5% in the VNP group.

Furthermore, T cells in the spleen and TdLNs are critical for antitumor responses, therefore we also analyzed the status of T cells in the spleen and TdLNs. As expected, CD69 expression of CD4⁺ T cells and CD8⁺ T cells was significantly increased in the spleen and TdLNs after VNP-IFN β administration compared with the other groups, which was consistent with the results of tumor-infiltrating T cells (Figures S6A–S6F). Notably, the proportions of PD1⁺ CD4⁺ T cells and PD1⁺ CD8⁺ T cells were reduced in the spleen compared to the PBS group, suggesting that immunosuppression was alleviated to some extent. (Figures S6G–S6I). Taken together, the above results suggest that VNP-IFN β can



Scheme 1. Schematic diagram of TME remodeling in B16F10 mice by VNP-IFN β

In short, VNP-IFN β was injected *i.v.* and penetrated in tumor site, inhibiting tumor progression subsequently. Specifically, VNP-IFN β penetrates through blood vessels to colonize the tumor. Due to bacterial proliferation, immune cells such as NEs, M ϕ s, and DCs are recruited into the tumor. Afterward, recombinant IFN β starts to be expressed and induces polarization of NEs and M ϕ s to an antitumor phenotype, which in turn promotes polarization of cDC2s. Finally, immunosuppression in the tumor gets relieved and cytotoxic CD4 $^+$ T cells are activated to exert antitumor effects.

activate DCs, which in turn activates antitumor immunity and relieves the tumor immunosuppression state, ultimately exerting metastasis suppression. Overall, we can conclude that VNP-IFN β can colonize and proliferate in hypoxic and/or necrotic regions caused by irregular blood vessels in tumor tissues after administration. Afterward, the accumulation of *Salmonella* in tumor tissues increases the penetration of host immune cells (i.e., NEs, M ϕ s, DCs). Subsequently, the IFN β expression plasmid carried within *Salmonella* began to express recombinant IFN β in the tumor, polarizing the infiltrating NEs and M ϕ s in the tumor to an antitumor phenotype and promoting the polarization of cDC2s.

Next, T cells infiltrated in tumor and peripheral tumor-associated immune organs were activated, immunosuppression in the tumor was relieved, and infiltrated cytotoxic CD4 $^+$ T cells were significantly increased. Eventually, this remodeling of the immune microenvironment caused by VNP-IFN β inhibited melanoma progression (Scheme 1).

DISCUSSION

NEs, the most abundant myeloid cells in human blood, are important regulators of cancer and have recently received increased attention in cancer. However, the role of NEs in cancer has long been a controversial issue. Some findings suggest that NEs exert protumor

Table 1. The tumor inhibition efficacy of VNP-IFN β in B16F10 subcutaneous xenograft model

Group	Tumor growth inhibition rates	Survival	TDT
PBS	0%	0%	1.85979
VNP	65.65%	75%	2.37550
VNP-IFN β	93.11%	95%	4.63452

functions, the first evidence for the pro-carcinogenic effect of NEs was that neutrophil-derived reactive oxygen species (ROS) amplify DNA damage during carcinogen exposure,⁴⁰ thereby promoting tumorigenesis. In addition, NEs support tumor cell proliferation through various paracrine signaling pathways, such as the release of prostaglandin E2 to promote cancer cell growth and the release of IL-1 receptor antagonist (IL-1RA) to counteract tumor cell senescence programs. Although NEs have been described as pro-tumorigenic in most studies, there is experimental evidence for an early antitumor effect of NEs. NEs can kill tumor cells through direct contact⁴⁶ and the generation of ROS or expression of NO,⁴⁷ TNF-related apoptosis inducing ligand (TRAIL)⁴⁸ and TNF α .⁴⁹ In conclusion, NEs have both pro-tumorigenic and anti-tumorigenic potential that reflects their plasticity in response to environmental cues.

Like TAMs, TANs also have different activation/differentiation states. Referring to the M1-M2 nomenclature for polarized M ϕ s, N1 and N2 are used to refer to antitumor and protumor NEs, respectively.⁸ NEs polarized into different phenotypes in response to cytokines in the TME, which provides an opportunity to remodel protumor NEs into antitumor NEs. It has been demonstrated that in the presence of IFN β NEs switch to an N1 phenotype, which is able to inhibit tumor growth and inhibit tumor seeding in the premetastatic lung,¹¹ suggesting that administration of IFN β may be a novel therapeutic strategy to remodel TANs for cancer therapy. In order to avoid first-pass effect and further improve bioavailability, intravenous administration is an important method for IFN β delivery.^{11,50} However, this conventional strategy only carries a limited dose of drug at a time, requires repeated administration and has the potential to cause systemic toxicity,¹³ thus we have turned our attention to tumor-targeting bacteria which can provide a steady supply of drugs.

The history of bacteria as anticancer therapeutic agents dates back to the mid-19th century, when William Coley used heat-inactivated *Streptococcus pyogenes* and *Serratia marcescens* to treat solid tumors.⁵¹ The specific targeting of attenuated *Salmonella* to various solid cancers makes it an ideal vector for the delivery and expression of therapeutic agents. To address the tumor-targeted delivery of IFN β , we utilized VNP20009 as a delivery vehicle, which have demonstrated its safety in patients with metastatic melanoma in a phase I clinical study.

Malignant melanoma, which is considered as “cold tumor”, does not respond to immunological checkpoint therapy due to poor infiltration of tumor-infiltrating lymphocytes and low tumor antigen mutations.^{52–54} In our scenario, proliferation of VNP-IFN β induces more neutrophil infiltration in tumor site, followed by recombinant IFN β stimulating neutrophil polarization to an N1 antitumor phenotype. This synergistic effect would remodel the immune microenvironment in the tumor, thereby inhibiting tumor progression. In this study, VNP-IFN β successfully colonized the tumor site and expressed IFN β , which significantly inhibited tumor growth and prolonged the survival of mice compared with VNP, furthermore, the tumor growth inhibition rate reached 93.11% and 81.934% in the B16F10 subcutaneous xenograft model (Table 1) and the B16F10 lung metastasis model (Table 2). In the B16F10 lung metastasis model, VNP-IFN β recruited more NEs and M ϕ s at the lung metastases and polarized them to an antitumor phenotype. Afterward, more DCs were recruited from the periphery and polarized to cDC2s phenotype to promote antigen presentation and activate CD4⁺ T cells-mediated antitumor immunity. Unfortunately, although VNP-IFN β exhibited satisfactory antitumor effects, the bacterial-induced hepatosplenomegaly did not resolve, and the elevated serum ALT and AST indicated the occurrence of liver injury. The tumor colonization rate of VNP needs to be further improved to minimize the side effects, and the balance between efficacy and safety of lysogenic bacteria needs to be further explored in the future.

Limitations of the study

In this manuscript, we constructed an expressed plasmid with constitutive promoter, which was an acceptable design in bacteria antitumor therapy field. However, owing to non-tumor-specific protein secretion, VNP-IFN β induced hepatosplenomegaly and weight loss. We next sought to design an expressed plasmid with inducible promoter or hypoxia promoter to enhance the tumor-specific expression and secretion of drug in tumor. In addition, we design a lysis circuit system based on VNP to ensure controllable the secretion of drug in tumor. We hope the above modifications could maintain the balance between therapeutic efficacy and safety.

Table 2. The tumor inhibition efficacy of VNP-IFN β in B16F10 lung metastasis model

Group	Tumor metastatic inhibition rates
PBS	0%
VNP	28.726%
VNP-IFN β	81.934%

STAR★METHODS

Detailed methods are provided in the online version of this paper and include the following:

- KEY RESOURCES TABLE
- RESOURCE AVAILABILITY
 - Lead contact
 - Materials availability
 - Data and code availability
- EXPERIMENTAL MODEL AND STUDY PARTICIPANT DETAILS
 - Bacterial strains and plasmid
 - Cell lines
 - Animals
- METHODS DETAILS
 - Animal treatments
 - Western Blot
 - Tumoral distribution of VNP-IFN β -mCherry and IFN β -mCherry
 - Bacterial titer of tumor
 - VNP-IFN β polarizes RAW264.7 cells to M1-like phenotype *in vitro*
 - Isolation of peritoneal NEs and bacterial stimulation
 - qPCR assay
 - Apoptosis detection by Annexin VPI staining
 - Flow cytometry
 - Statistical analysis

SUPPLEMENTAL INFORMATION

Supplemental information can be found online at <https://doi.org/10.1016/j.isci.2024.109372>.

ACKNOWLEDGMENTS

This work was supported by the grants from the National Natural Science Foundation of China of China (82130106 , 32250016), Nanjing Special Fund for Life and Health Science and Technology (202110016, China), Changzhou Bureau of Science and Technology (CJ20210024, CZ20210010, CJ20220019, China) and Jiangsu TargetPharma Laboratories Inc., China.

AUTHOR CONTRIBUTIONS

L.N.L. and Q.L. designed and performed most *in vitro* and *in vivo* experiments. C.C. and W.J.X. designed some *in vitro* and *in vivo* experiments and flow cytometry analyses and conducted the microscopy studies. C.H. provided clinical and preclinical guidance. All authors contributed to the conception of the study, the analysis of the data, and the revision of the manuscript.

DECLARATION OF INTERESTS

The authors declare no competing interests.

Received: October 2, 2023

Revised: January 16, 2024

Accepted: February 26, 2024

Published: March 2, 2024

REFERENCES

1. Pitt, J.M., Marabelle, A., Eggermont, A., Soria, J.C., Kroemer, G., and Zitvogel, L. (2016). Targeting the tumor microenvironment: removing obstruction to anticancer immune responses and immunotherapy. *Ann. Oncol.* 27, 1482–1492.
2. Sharma, P., and Allison, J.P. (2015). The future of immune checkpoint therapy. *Science* 348, 56–61.
3. Fukumura, D., Kloepper, J., Amoozgar, Z., Duda, D.G., and Jain, R.K. (2018). Enhancing cancer immunotherapy using antiangiogenics: opportunities and challenges. *Nat. Rev. Clin. Oncol.* 15, 325–340.
4. Cassetta, L., and Pollard, J.W. (2018). Targeting macrophages: therapeutic approaches in cancer. *Nat. Rev. Drug Discov.* 17, 887–904.
5. Xiao, Y., and Yu, D. (2021). Tumor microenvironment as a therapeutic target in cancer. *Pharmacol. Ther.* 221, 107753.
6. Kargl, J., Busch, S.E., Yang, G.H.Y., Kim, K.H., Hanke, M.L., Metz, H.E., Hubbard, J.J., Lee, S.M., Madtes, D.K., McIntosh, M.W., and Houghton, A.M. (2017). NEs dominate the immune cell composition in non-small cell lung cancer. *Nat. Commun.* 8, 14381.
7. Jaillon, S., Ponzetta, A., Di Mitri, D., Santoni, A., Bonecchi, R., and Mantovani, A. (2020). Neutrophil diversity and plasticity in tumour progression and therapy. *Nat. Rev. Cancer* 20, 485–503.
8. Fridlender, Z.G., Sun, J., Kim, S., Kapoor, V., Cheng, G., Ling, L., Worthen, G.S., and Albelda, S.M. (2009). Polarization of

- tumor-associated neutrophil phenotype by TGF-beta: "N1" versus "N2" TAN. *Cancer Cell* 16, 183–194.
9. Mittendorf, E.A., Alatrash, G., Qiao, N., Wu, Y., Sukhmalchandra, P., St John, L.S., Philips, A.V., Xiao, H., Zhang, M., Ruisaard, K., et al. (2012). Breast cancer cell uptake of the inflammatory mediator neutrophil elastase triggers an anticancer adaptive immune response. *Cancer Res.* 72, 3153–3162.
 10. Granot, Z., Henke, E., Comen, E.A., King, T.A., Norton, L., and Benezra, R. (2011). Tumor entrained NEs inhibit seeding in the premetastatic lung. *Cancer Cell* 20, 300–314.
 11. Andzinski, L., Kasnitz, N., Stahnke, S., Wu, C.F., Gereke, M., von Köckritz-Blickwede, M., Schilling, B., Brandau, S., Weiss, S., and Jablonska, J. (2016). Type I IFNs induce anti-tumor polarization of tumor associated NEs in mice and human. *Int. J. Cancer* 138, 1982–1993.
 12. Wu, C.F., Andzinski, L., Kasnitz, N., Kröger, A., Klawonn, F., Lienenklaus, S., Weiss, S., and Jablonska, J. (2015). The lack of type I interferon induces neutrophil-mediated pre-metastatic niche formation in the mouse lung. *Int. J. Cancer* 137, 837–847.
 13. Han, C., Zhang, X., Pang, G., Zhang, Y., Pan, H., Li, L., Cui, M., Liu, B., Kang, R., Xue, X., et al. (2022). Hydrogel microcapsules containing engineered bacteria for sustained production and release of protein drugs. *Biomaterials* 287, 121619.
 14. Pechenov, S., Bhattacharjee, H., Yin, D., Mittal, S., and Subramony, J.A. (2017). Improving drug-like properties of insulin and GLP-1 via molecule design and formulation and improving diabetes management with device & drug delivery. *Adv. Drug Deliv. Rev.* 112, 106–122.
 15. Mehrotra, S., Lynam, D., Maloney, R., Pawelec, K.M., Tuszyński, M.H., Lee, I., Chan, C., and Sakamoto, J. (2010). Time Controlled Protein Release from Layer-by-Layer Assembled Multilayer Functionalized Agarose Hydrogels. *Adv. Funct. Mater.* 20, 247–258.
 16. Wu, L., Bao, F., Li, L., Yin, X., and Hua, Z. (2022). Bacterially mediated drug delivery and therapeutics: Strategies and advancements. *Adv. Drug Deliv. Rev.* 187, 114363.
 17. Wu, L., Li, L., Li, S., Liu, L., Xin, W., Li, C., Yin, X., Xu, X., Bao, F., and Hua, Z. (2022). Macrophage-mediated tumor-targeted delivery of engineered Salmonella typhimurium VNP20009 in anti-PD1 therapy against melanoma. *Acta Pharm. Sin. B* 12, 3952–3971.
 18. Liu, L., Liu, X., Xin, W., Zhou, L., Huang, B., Han, C., Cao, Z., and Hua, Z. (2023). A bacteria-based system expressing anti-TNF- α nanobody for enhanced cancer immunotherapy. *Signal Transduct. Target. Ther.* 8, 134.
 19. Jia, L.J., Xu, H.M., Ma, D.Y., Hu, Q.G., Huang, X.F., Jiang, W.H., Li, S.F., Jia, K.Z., Huang, Q.L., and Hua, Z.C. (2005). Enhanced therapeutic effect by combination of tumor-targeting Salmonella and endostatin in murine melanoma model. *Cancer Biol. Ther.* 4, 840–845.
 20. Yoon, W., Park, Y.C., Kim, J., Chae, Y.S., Byeon, J.H., Min, S.H., Park, S., Yoo, Y., Park, Y.K., and Kim, B.M. (2017). Application of genetically engineered Salmonella typhimurium for interferon-gamma-induced therapy against melanoma. *Eur. J. Cancer* 70, 48–61.
 21. Jiang, S.N., Park, S.H., Lee, H.J., Zheng, J.H., Kim, H.S., Bom, H.S., Hong, Y., Szardenings, M., Shin, M.G., Kim, S.C., et al. (2013). Engineering of bacteria for the visualization of targeted delivery of a cytolytic anticancer agent. *Mol. Ther.* 21, 1985–1995.
 22. Chen, J., Yang, B., Cheng, X., Qiao, Y., Tang, B., Chen, G., Wei, J., Liu, X., Cheng, W., Du, P., et al. (2012). Salmonella-mediated tumor-targeting TRAIL gene therapy significantly suppresses melanoma growth in mouse model. *Cancer Sci.* 103, 325–333.
 23. Zheng, J.H., Nguyen, V.H., Jiang, S.N., Park, S.H., Tan, W., Hong, S.H., Shin, M.G., Chung, I.J., Hong, Y., Bom, H.S., et al. (2017). Two-step enhanced cancer immunotherapy with engineered Salmonella typhimurium secreting heterologous flagellin. *Sci. Transl. Med.* 9, eaak9537.
 24. al-Ramadi, B.K., Fernandez-Cabezudo, M.J., El-Hasasna, H., Al-Salam, S., Bashir, G., and Chouaib, S. (2009). Potent anti-tumor activity of systemically-administered IL2-expressing Salmonella correlates with decreased angiogenesis and enhanced tumor apoptosis. *Clin Immunol* 130, 89–97.
 25. Ye, J., Li, L., Zhang, Y., Zhang, X., Ren, D., and Chen, W. (2013). Recombinant Salmonella-based 4-1BBL vaccine enhances T cell immunity and inhibits the development of colorectal cancer in rats: in vivo effects of vaccine containing 4-1BBL. *J. Biomed. Sci.* 20, 8.
 26. Zhang, L., Gao, L., Zhao, L., Guo, B., Ji, K., Tian, Y., Wang, J., Yu, H., Hu, J., Kalvakolanu, D.V., et al. (2007). Intratumoral delivery and suppression of prostate tumor growth by attenuated Salmonella enterica serovar typhimurium carrying plasmid-based small interfering RNAs. *Cancer Res.* 67, 5859–5864.
 27. Vitale, I., Manic, G., Coussens, L.M., Kroemer, G., and Galluzzi, L. (2019). Macrophages and Metabolism in the Tumor Microenvironment. *Cell Metab.* 30, 36–50.
 28. Lizotte, P.H., Baird, J.R., Stevens, C.A., Lauer, P., Green, W.R., Brockstedt, D.G., and Fiering, S.N. (2014). Attenuated *Listeria monocytogenes* reprograms M2-polarized tumor-associated macrophages in ovarian cancer leading to iNOS-mediated tumor cell lysis. *Oncol Immunology* 3, e28926.
 29. Ghambashidze, K., Chikhladze, R., Saladze, T., Hoopes, P.J., and Shubitidze, F. (2023). *E. coli* Phageslate: A Primer to Enhance Nanoparticles and Drug Deliveries in Tumor. *Cancers* 15, 2315.
 30. Dai, X., Lu, L., Deng, S., Meng, J., Wan, C., Huang, J., Sun, Y., Hu, Y., Wu, B., Wu, G., et al. (2020). USP7 targeting modulates anti-tumor immune response by reprogramming Tumor-associated Macrophages in Lung Cancer. *Theranostics* 10, 9332–9347.
 31. Pan, J., Li, X., Shao, B., Xu, F., Huang, X., Guo, X., and Zhou, S. (2022). Self-Blockade of PD-L1 with Bacteria-Derived Outer-Membrane Vesicle for Enhanced Cancer Immunotherapy. *Adv. Mater.* 34, e2106307.
 32. Chen, G., Wei, D.P., Jia, L.J., Tang, B., Shu, L., Zhang, K., Xu, Y., Gao, J., Huang, X.F., Jiang, W.H., et al. (2009). Oral delivery of tumor-targeting Salmonella exhibits promising therapeutic efficacy and low toxicity. *Cancer Sci.* 100, 2437–2443.
 33. Cheng, X., Zhang, X., Zhou, Y., Zhang, C., and Hua, Z.C. (2014). A Salmonella Typhimurium mutant strain capable of RNAi delivery: higher tumor-targeting and lower toxicity. *Cancer Biol. Ther.* 15, 1068–1076.
 34. Makuch, E., Jasyk, I., Kula, A., Lipiński, T., and Siednienko, J. (2022). IFN β -Induced CXCL10 Chemokine Expression Is Regulated by Pellino3 Ligase in Monocytes and Macrophages. *Int. J. Mol. Sci.* 23.
 35. Goebel, M.U., Baase, J., Pithan, V., Exton, M., Saller, B., Schedlowski, M., and Limmroth, V. (2002). Acute interferon beta-1b administration alters hypothalamic-pituitary-adrenal axis activity, plasma cytokines and leukocyte distribution in healthy subjects. *Psychoneuroendocrinology* 27, 881–892.
 36. Jablonska, J., Leschner, S., Westphal, K., Lienenklaus, S., and Weiss, S. (2010). NEs responsive to endogenous IFN-beta regulate tumor angiogenesis and growth in a mouse tumor model. *J. Clin. Invest.* 120, 1151–1164.
 37. Mi, Z., Guo, L., Liu, P., Qi, Y., Feng, Z., Liu, J., He, Z., Yang, X., Jiang, S., Wu, J., et al. (2021). Trojan Horse* Salmonella Enabling Tumor Homing of Silver Nanoparticles via Neutrophil Infiltration for Synergistic Tumor Therapy and Enhanced Biosafety. *Nano Lett.* 21, 414–423.
 38. Shen, M., Hu, P., Donskov, F., Wang, G., Liu, Q., and Du, J. (2014). Tumor-associated NEs as a new prognostic factor in cancer: a systematic review and meta-analysis. *PLoS One* 9, e98259.
 39. Shaul, M.E., and Fridlender, Z.G. (2019). Tumor-associated NEs in patients with cancer. *Nat. Rev. Clin. Oncol.* 16, 601–620.
 40. Knaapen, A.M., Seiler, F., Schilderman, P.A., Nehls, P., Bruch, J., Schins, R.P., and Borm, P.J. (1999). NEs cause oxidative DNA damage in alveolar epithelial cells. *Free Radic. Biol. Med.* 27, 234–240.
 41. Broz, M.L., Binnewies, M., Boldajipour, B., Nelson, A.E., Pollack, J.L., Erle, D.J., Barczak, A., Rosenblum, M.D., Daud, A., Barber, D.L., et al. (2014). Dissecting the tumor myeloid compartment reveals rare activating antigen-presenting cells critical for T cell immunity. *Cancer Cell* 26, 938.
 42. Wculek, S.K., Cueto, F.J., Mujal, A.M., Melero, I., Krummel, M.F., and Sancho, D. (2020). Dendritic cells in cancer immunology and immunotherapy. *Nat. Rev. Immunol.* 20, 7–24.
 43. Salmon, H., Idoyaga, J., Rahman, A., Leboeuf, M., Remark, R., Jordan, S., Casanova-Acebes, M., Khudoynazarova, M., Agudo, J., Tung, N., et al. (2016). Expansion and Activation of CD103(+) Dendritic Cell Progenitors at the Tumor Site Enhances Tumor Responses to Therapeutic PD-L1 and BRAF Inhibition. *Immunity* 44, 924–938.
 44. Binnewies, M., Mujal, A.M., Pollack, J.L., Combes, A.J., Hardison, E.A., Barry, K.C., Tsui, J., Ruhland, M.K., Kersten, K., Abushawish, M.A., et al. (2019). Unleashing Type-2 Dendritic Cells to Drive Protective Antitumor CD4(+) T Cell Immunity. *Cell* 177, 556–571.e16.
 45. Cibrián, D., and Sánchez-Madrid, F. (2017). CD69: from activation marker to metabolic gatekeeper. *Eur. J. Immunol.* 47, 946–953.
 46. Blaisdell, A., Crequer, A., Columbus, D., Daikoku, T., Mittal, K., Dey, S.K., and Erlebacher, A. (2015). NEs Oppose Uterine Epithelial Carcinogenesis via Debridement of Hypoxic Tumor Cells. *Cancer Cell* 28, 785–799.
 47. Mahiddine, K., Blaisdell, A., Ma, S., Créquer-Grandhomme, A., Lowell, C.A., and Erlebacher, A. (2020). Relief of tumor hypoxia

- unleashes the tumoricidal potential of NEs. *J. Clin. Invest.* *130*, 389–403.
48. Koga, Y., Matsuzaki, A., Suminoe, A., Hattori, H., and Hara, T. (2004). Neutrophil-derived TNF-related apoptosis-inducing ligand (TRAIL): a novel mechanism of antitumor effect by NEs. *Cancer Res.* *64*, 1037–1043.
49. Finisguerra, V., Di Conza, G., Di Matteo, M., Serneels, J., Costa, S., Thompson, A.A.R., Wauters, E., Walmsley, S., Prenen, H., Granot, Z., et al. (2015). MET is required for the recruitment of anti-tumoural NEs. *Nature* *522*, 349–353.
50. Zhang, Y., Zhang, H., Ghosh, D., and Williams, R.O. (2020). 3rd, Just how prevalent are peptide therapeutic products? A critical review. *Int. J. Pharm.* *587*, 119491.
51. Guo, Y., Chen, Y., Liu, X., Min, J.J., Tan, W., and Zheng, J.H. (2020). Targeted cancer immunotherapy with genetically engineered oncolytic *Salmonella typhimurium*. *Cancer Lett.* *469*, 102–110.
52. Binnewies, M., Roberts, E.W., Kersten, K., Chan, V., Fearon, D.F., Merad, M., Coussens, L.M., Gaboritovitch, D.I., Ostrand-Rosenberg, S., Hedrick, C.C., et al. (2018). Understanding the tumor immune microenvironment (TIME) for effective therapy. *Nat. Med.* *24*, 541–550.
53. Galon, J., and Bruni, D. (2019). Approaches to treat immune hot, altered and cold tumours with combination immunotherapies. *Nat. Rev. Drug Discov.* *18*, 197–218.
54. Huang, L., Li, Y., Du, Y., Zhang, Y., Wang, X., Ding, Y., Yang, X., Meng, F., Tu, J., Luo, L., and Sun, C. (2019). Mild photothermal therapy potentiates anti-PD-L1 treatment for immunologically cold tumors via an all-in-one and all-in-control strategy. *Nat. Commun.* *10*, 4871.
55. Liu, L., Xin, W., Li, Q., Huang, B., Yin, T., Hua, S., Yang, C., Chen, C., Han, C., and Hua, Z. (2023). Neutrophil-Mediated Tumor-Targeting Delivery System of Oncolytic Bacteria Combined with ICB for Melanoma Lung Metastasis Therapy. *Adv. Sci.* *10*, e2301835.

STAR★METHODS

KEY RESOURCES TABLE

REAGENT or RESOURCE	SOURCE	IDENTIFIER
Antibodies		
Ms CD45-PE Cy7	BD Pharmingen™	Cat# 552848; RRID: AB_394489
Ms CD8a-PerCP Cy5.5	BD Pharmingen™	Cat# 5551162; RRID: AB_394081
Ms CD8-FITC	BD Pharmingen™	Cat# 5553030; RRID: AB_394568
Ms CD11c-PE	BD Pharmingen™	Cat# 5553802; RRID: AB_396684
Ms I-A/I-E BB700	BD Pharmingen™	Cat# 5746197; RRID: AB_2743461
Ms CD11b- PerCP Cy5.5	BD Pharmingen™	Cat# 5550993; RRID: AB_394002
Ms CD11b- APC	BD Pharmingen™	Cat# 5557396; RRID: AB_398535
Ms CD80-BV421	BD Pharmingen™	Cat# 5562611; RRID: AB_2737675
Ms CD206-AF647	BD Pharmingen™	Cat# 5565250; RRID: AB_2739133
Ms CD69-BV421	BD Pharmingen™	Cat# 5562920; RRID: AB_2687422
Ms F4/80-BV510	BD Pharmingen™	Cat# 5743280; RRID: AB_2741398
Ms Ly6C-PE	BD Pharmingen™	Cat# 5560592; RRID: AB_1727556
Ms Ly6G-PE.Cy7	BD Pharmingen™	Cat# 5560601; RRID: AB_1727562
CD4-PE.Cy7	eBioscience™	Cat# 512-0043-82; RRID: AB_469576
Granzyme B-PE	eBioscience™	Cat# 512-8898-82; RRID: AB_10870787
PD1-APC	eBioscience™	Cat# 517-9985-82; RRID: AB_11149358
TNF α -BV421	Biolegend™	Cat# 5506328; RRID: AB_2562902
CD86-FITC	Biolegend™	Cat# 5105109; RRID: AB_313162
CD103-PE.Cy7	Biolegend™	Cat# 5121426; RRID: AB_2563691
Bacterial and virus strains		
VNP20009	The Nanjing University	N/A
VNP- IFN β	The Nanjing University	N/A
Biological samples		
Spleen, blood, lymph nodes	Mouse	N/A
Chemicals, peptides, and recombinant proteins		
DMEM	BBI	Cat# E600003-0500
1640	BBI	Cat# E6000028
Fetal bovine serum (FBS)	HyClone	Cat# SH30070
Trypsin-EDTA (0.25%)	Servicebio	Cat# G4011-100ML
OCT embedding agent	Servicebio	Cat# G6059-110ML
Triton X-100	Sigma	Cat# 9036-19-5
blood cell lysis buffer	Servicebio	Cat# G2015-500ML
Critical commercial assays		
ClonExpress II/MultiS One Step Cloning Kit	Vazyme	Cat# C112/C113
Trizol reagent	Invitrogen	Cat# 15596026
ReverTra Ace® qPCR RT Kit	Toyobo	Cat# FSQ-101
AceQ® qPCR SYBR® Green Master Mix	Vazyme	Cat# Q111-02
Software and algorithms		
GraphPad Prism	GraphPad Software	RRID:SCR_002798
FlowJo	BD	flowjo.com
ImageJ	ImageJ	ImageJ.net

RESOURCE AVAILABILITY

Lead contact

Further information and requests for resources and reagents should be directed to and will be fulfilled by the lead contact Zichun Hua (zchua@nju.edu.cn).

Materials availability

This study did not generate new unique reagents.

Data and code availability

- All data reported in this paper will be shared by the [lead contact](#) upon request.
- This paper does not report original code.
- Any additional information required to reanalyze the data reported in this paper is available from the [lead contact](#) upon request.

EXPERIMENTAL MODEL AND STUDY PARTICIPANT DETAILS

Bacterial strains and plasmid

VNP20009 (VNP) and VNP20009 expressed IFN β with J23100 promoter initiation (VNP-IFN β) were cultured in Luria Bertani (LB) broth or on LB agar plates at 37°C. Bacteria growth curve was measured by the microplate reader constantly. All plasmids were constructed by using the ClonExpress II/MultiS One Step Cloning Kit (C112/C113, Vazyme). The morphogens of bacteria were detected by scanning electron microscopy (SEM). When OD₆₀₀ reached 0.6–0.8 (logarithmic phase), measured the expression of the protein in bacteria by sonication lysis bacteria.

Cell lines

The B16F10 cells (mouse melanoma cell) and RAW 264.7 (mouse macrophage cell) were stored in our lab. B16F10 cells were both cultured in RPMI-1640 medium (BBI, China) containing 10% fetal bovine serum (FBS) (HyClone, USA). RAW 264.7 cells were cultured in Dulbecco's modified Eagle's medium (DMEM) (BBI, China) containing 15% FBS (Gibco, USA). All the cell lines were cultured at 37°C in an incubator with 5% CO₂.

Animals

Female C57BL/6 and BALB/c, 6 to 8 weeks old, were purchased from Huachuang Sino Company (Nanjing, China) and kept under specific pathogen-free conditions. All animal experiments were approved by Nanjing University Institutional Animal Care and Use Committee (IACUC-2003167).

METHODS DETAILS

Animal treatments

We established B16F10 lung metastases model and subcutaneous xenograft model. In brief, 2×10^5 B16F10 cells re-suspended in 100 μ L of PBS were intravenous (*i.v.*) injected to establish lung metastases model. 3 days after lung metastases model establishment, PBS, 1×10^6 CFU VNP and 1×10^6 CFU VNP-IFN β was injected by tail vein (*i.v.*) into tumor-bearing mice respectively. Then 7 days after administration, executed the mice and collected tumor, spleen, tumor-draining lymph nodes (TdLNs), and peripheral blood. Whole peripheral blood samples were collected to detect aspartate aminotransferase (AST), alanine aminotransferase (ALT), creatinine (Scr), and blood urea nitrogen (BUN). Mouse organs were collected for H&E staining. These experiments were completed by Wuhan servicebio technology company (Wuhan, China).

To establish subcutaneous xenograft model, 1×10^6 B16F10 cells re-suspended in 0.1 mL PBS, were injected subcutaneously on the mid-right flank. 7 days after B16F10 cells inoculation, PBS, 1×10^6 CFU VNP and 1×10^6 CFU VNP-IFN β was injected respectively by *i.v.* injection into the tumor-bearing mice. The mice were weighed daily after administration and the date of death was recorded to plot the survival curve.

The tumor growth inhibition rates (15 Days) were calculated as follows: tumor inhibition rate = (1-average tumor volume of the treatment group/average tumor volume of control group) \times 100. To comply with ethical requirements, the animal experiments, some of the control groups (PBS group, VNP group) were combined with our previous work, which has been published online under the name of "Neutrophil-Mediated Tumor-Targeting Delivery System of Oncolytic Bacteria Combined with ICB for Melanoma Lung Metastasis Therapy".⁵⁵

Western Blot

Bacteria were harvested as they grew to the logarithmic phase and disrupted by ultrasound and the supernatants were collected. All protein samples were subjected to 12% SDS-polyacrylamide gel electrophoresis and then transferred to PVDF membranes. The western blot antibody used was as follows: ANTI-FLAGM2 antibody (B3111-1MG) from Sigma (USA).

Tumoral distribution of VNP-IFN β -mCherry and IFN β -mCherry

PBS, 1×10^7 CFU VNP-IFN β -mCherry and $6\mu\text{g}$ IFN β -mCherry was injected respectively by *i.v.* injection into the subcutaneous xenograft model mice. Then executed the mice and collected tumor at different time. Afterward, the tumors were fixed in 4% paraformaldehyde solution for 24 h at 4°C, followed by dehydration by adding 30% sucrose solution for 24h, and then the tumors were wrapped with OCT embedding agent (Servicebio G6059-110ML). then the tumor was sectioned with Leica CM1950 cryosections.

Bacterial titer of tumor

3 days after administration, subcutaneous tumor and organs were collected and shredded with scissors, lysed using 1% Triton X-100 in PBS at 1 h at 4°C. The supernatants were planted on LB agar after being diluted in PBS, and the bacterial numbers were calculated.

VNP-IFN β polarizes RAW264.7 cells to M1-like phenotype *in vitro*

4×10^5 RAW264.7 cells were seeded in 6-well plates. Then VNP-IFN β (MOI = 100:1) or not was added to each well and incubation for 1.5 h. Cells were collected for FACS and qPCR assay.

Isolation of peritoneal NEs and bacterial stimulation

The mice used to extract NEs belonged to the same batch as the line selected in the pharmacodynamics experiment. 4–6 h before isolation of peritoneal NEs, mice were subcutaneously (*s.c.*) injected with 1 mL nutrient broth to stimulate peritoneal NEs maturity. NEs were isolated using a Percoll gradient and identified by FACS, then plated at a density of 1×10^6 cells mL^{-1} . Then VNP and 1×10^6 VNP-IFN β (MOI = 100:1) were added and incubated together for 1.5h and then RNA was extracted for qPCR.

qPCR assay

Total RNA was isolated with Trizol reagent (Invitrogen). cDNA was generalized using ReverTra Ace qPCR RT Kit (Toyobo). qPCR was done with primers (detailed sequence information is provided in below table to determine the mRNA expression level of the target gene. qPCR was performed on StepOne Real-Time PCR System (Applied Biosystems, USA) with AceQ qPCR SYBR Green Master Mix (Vazyme China). Data were analyzed by StepOne Software 2.1 (Applied Biosystems, USA) according to the manufacturer's specifications. 18S rRNA was used as a control.

The primer sequence of RT-PCR

Primer	Forward (5'-3')	Reverse (5'-3')
18s	GTAACCCGTTGAACCCATT	CCATCCAATCGGTAGTAGCG
IFN- γ	GCCACGGCACAGTCATTGA	TGCTGATGGCCTGATTGTCTT
TNF- α	ACCACGCTCTTCTGTCTACT	AGGAGGTTGACTTTCTCCTG
iNos	GTTCTCAGCCCAACAATAACAAGA	GTGGACGGGTGCGATGCAC
Arg-1	GATTGGCAAGGTGATGGAAG	TCAGTCCCTGGCTTATGGTT
IL-1 β	GAAATGCCACCTTTTGACAGTG	TGGATGCTCTCATCAGGACAG
Fizz1	CCAATCCAGCTAACTATCCCTCC	CCAGTCAACGAGTAAGCACAG
TGF- β	CTCCCGTGGCTTCTAGTGC	GCCTTAGTTTGGACAGGATCTG
CCL3	ACCATGACACTCTGCAACCA	TCAGGCATTTCAGTCCAGGT
iCAM1	GAAGCTTCTTTTGCTCTGCC	AGCAGTACTGGCACCAGAAT
CCL2	CAGGTCCCTGTCATGCTTCT	GTCAGCACAGACCTCTCTCT

Apoptosis detection by Annexin V/PI staining

B16F10 cells were seeded in 24-well plates at a density of 2×10^5 per well and incubated with different bacteria or bacteria-stimulated RAW264.7 cell supernatant for 16h. Apoptosis levels of B16F10 cells were determined using a kit developed in our lab. 1 μL Annexin V-APC (1 mg/mL) and 1 μL propidium-PE (PI, 1 mg/mL) were incubated with cells in binding buffer for 30 min at 4°C. Stained cells were analyzed using FACS (NovoCyte Flow Cytometer (ACEA®)). The results were analyzed using FlowJo VX software.

Flow cytometry

5 days after administration, tumor-bearing mouse tissues were collected. Spleen and TdLNs were homogenized with 1 mL PBS to obtain single-cell suspensions. Peripheral blood lymphocytes were obtained from peripheral blood. Tumors on the lung were shredded and then digested with mixed medium (1 mg/mL Collagenase I, 1 mg/mL Collagenase IV, 200 $\mu\text{g}/\text{mL}$ DNase I) at 37°C for 40min. All tissues were lysed

with red blood cell lysis buffer (Beyotime, Nanjing), and then the cell suspensions were passed through a 200-mesh filter. The single-cell suspensions were incubated in 1% BSA for 15 min at 4°C and stained with the following antibodies for 30 min at 4°C (detailed antibody information is provided in below table). The stained cells were analyzed using flow cytometer (BD@ FACS Canto II systems). The results were analyzed using FlowJo VX software.

The information of FACs antibody		
Antibodies	Article No.	Company
Ms CD45-PE Cy7	552848	BD Pharmingen™
Ms CD8a-PerCP Cy5.5	551162	BD Pharmingen™
Ms CD8-FITC	553030	BD Pharmingen™
Ms CD11c-PE	553802	BD Pharmingen™
Ms I-A/I-E BB700	746197	BD Pharmingen™
Ms CD11b- PerCP Cy5.5	550993	BD Pharmingen™
Ms CD11b- APC	557396	BD Pharmingen™
Ms CD80-BV421	562611	BD Pharmingen™
Ms CD206-AF647	565250	BD Pharmingen™
Ms CD69-BV421	562920	BD Pharmingen™
Ms F4/80-BV510	743280	BD Pharmingen™
Ms Ly6C-PE	560592	BD Pharmingen™
Ms Ly6G-PE.Cy7	560601	BD Pharmingen™
CD4-PE.Cy7	12-0043-82	eBioscience™
Granzyme B-PE	12-8898-82	eBioscience™
PD1-APC	17-9985-82	eBioscience™
TNF α -BV421	506328	Biolegend™
CD86-FITC	105005	Biolegend™
CD103-PE.Cy7	121426	Biolegend™

Statistical analysis

Results are expressed as the mean \pm SD as specified. Mean differences were compared using t-test or one-way ANOVA. A value of $p < 0.05$ was regarded as statistically significant. Data were analyzed with GraphPad Prism 8.3 software. (Data are shown as the mean \pm SD. **** $p < 0.0001$, *** $p < 0.001$, ** $p < 0.01$, * $p < 0.05$, ns: no significance.)